ACS Catalysis

Research Article

pubs.acs.org/acscatalysis

Computational Evidence for the Catalytic Mechanism of Human Glutathione S-Transferase A3-3: A QM/MM Investigation

Matteo Calvaresi,[†] Marco Stenta,*[,‡] Marco Garavelli,[†] Piero Altoé,[†] and Andrea Bottoni*[,†]

[†]Dipartimento di Chimica "G. Ciamician", Università di Bologna, via Selmi 2, 40126 Bologna, Italy

[‡]Laboratory for Biomolecular Modeling, Institute of Bioengineering, School of Life Sciences, Ecole Polytechnique Fédérale de Lausanne (EPFL), CH-1015 Lausanne, Switzerland

Supporting Information

ABSTRACT: A Quantum Mechanics/Molecular Mechanics (QM/MM) computational investigation of the catalytic mechanism of the human glutathione transferase A3-3 (hGSTA3-3) has been carried out. The results demonstrate that the isomerization reaction is concerted, but highly asynchronous: in the first reaction phase the glutathione (GSH) negative sulfur (thiolate) acts as a base and deprotonates carbon C4 of the substrate Δ^5-androstene-3,17-dione (Δ^5-AD); in the second reaction phase the hydroxyl proton of the tyrosine fragment Y9 is transferred to C6 affording the Δ^4-androstene-3,17-dione product (Δ^4-AD). The initial state of the enzyme is subsequently restored by transferring a proton from the GSH sulfur to the tyrosine negative oxygen. There is no evidence for a "genuine" stepwise mechanism involving the formation of a real dienolate intermediate as suggested in previous papers. Furthermore, our computations have evidenced that, when we consider the whole process (including the restoring of the enzyme), GSH behaves as a base/acid catalyst (as hypothesized by some authors), but it requires the participation of the tyrosine Y9 acting as a proton shuttle. A "fingerprint analysis" has been used to rank the electrostatic effects on the catalysis of the various residues surrounding the active site. This analysis highlights the role played by the arginine residue R15 in stabilizing the initial complex in agreement with previous suggestions based on crystal structures.

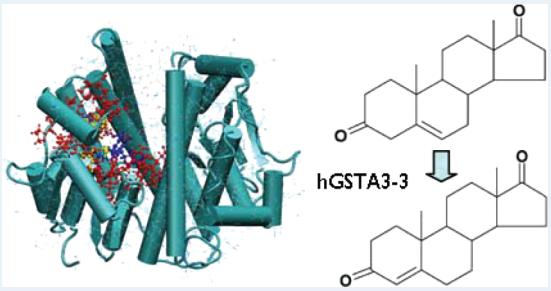

KEYWORDS: *QM/MM calculations, human glutathione transferase A3-3, isomerization reaction, computational chemistry, enzymatic mechanism*

INTRODUCTION

Glutathione transferases (GSTs) belong to a family of enzymes (formed by several gene classes) which play an important role in detoxification reactions of mutagenic and carcinogenic electrophiles by catalyzing the conjugation of these substances to glutathione (GSH).[1,2] In addition to this function some GSTs play a key-role in the steroid hormone biosynthesis which starts from cholesterol and proceeds through a multiple step process involving oxidation and isomerization.[3] In particular the human GST A3-3 (hGSTA3-3) catalyzes the isomerization of Δ^5-androstene-3,17-dione (Δ^5-AD) into Δ^4-androstene-3,17-dione (Δ^4-AD), a process representing a crucial step in the biosynthesis of steroid hormones such as testosterone and progesterone.[4−6] It has been demonstrated that this catalytic activity is governed by a small number of active site residues that distinguish hGSTA3-3 from other members of the same class such as hGSTA1−1 and hGSTA2−2 showing almost negligible isomerase activity.[5,6]

A few years ago Ji and co-workers determined the crystal structure of hGSTA3-3 in complex with glutathione (GSH).[7] GSH, which behaves as a cofactor, is bound to the G-site (GSH-binding site) by a network of hydrogen bonds, as previously shown for hGSTA1−1.[8] Using the crystal structure of hGSTA3-3·GSH, these authors docked the substrate Δ^5-AD into the active site of the enzyme (formed by two subunits) and constructed a model of the hGSTA3-3·GSH·Δ^5-AD ternary complex. Using this model and available biochemical data, they proposed the catalytic mechanism shown in Scheme 1. In this mechanism the sulfur of GSH is ionized (thiolate) and acts as a base to withdraw a proton from C4 of Δ^5-AD. This would lead to the formation of a dienolate intermediate where the negative charge is strongly delocalized along the O−C3−C4−C5-C6 conjugate system. This charge delocalization allows the transfer of a proton from the OH group of tyrosine (Y9) to C6 affording the Δ^4-AD product. In a subsequent step of the catalytic process the proton of GSH is transferred to the Y9 ionized hydroxyl group, thus restoring the initial state of the enzyme which, after product release, is ready to accept a new Δ^5-AD molecule. Previous studies have already established that the sulfur of GSH, in a complex with GST, must be ionized and that the Y9 residue must be protonated.[6]

Very recently Mannervick and co-workers[9] determined for the first time the crystal structure of GST A3-3 in complex with GSH and the product of the steroid isomerization Δ^4-AD.

Received: July 14, 2011
Revised: December 14, 2011
Published: January 10, 2012

Scheme 1. Proposed Catalytic Mechanism for hGSTA3-3

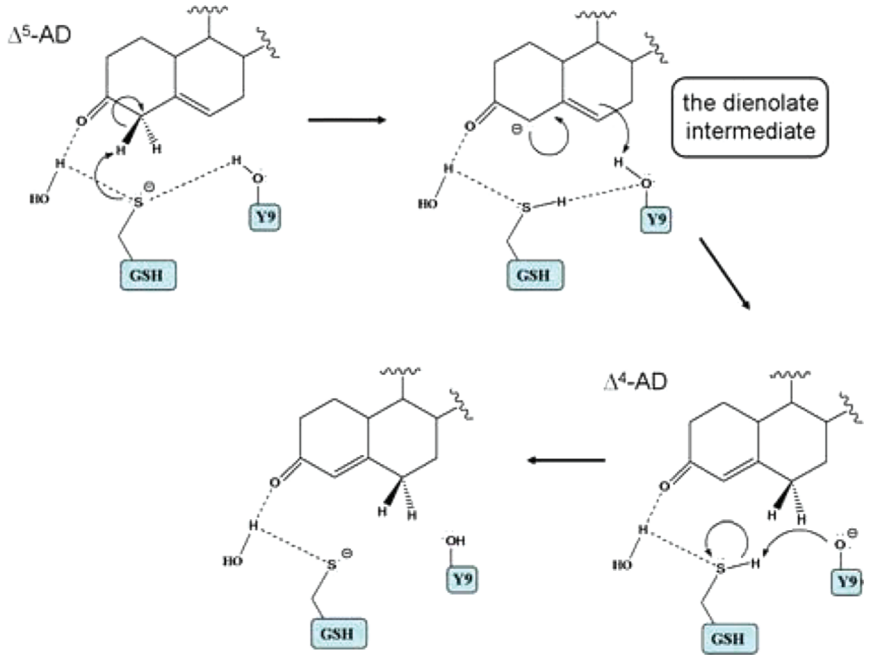

These authors propose a different mechanism where GSH acts as an acid/base catalyst affording the proton transfer from C4 to C6, similarly to what was suggested in a previous work.[6] To justify the experimental evidence showing the prominent role of the tyrosine residue Y9 in the catalysis, they proposed that tyrosine assists the proton transfer to C6 via a hydrogen bond with the protonated sulfur of GSH. Following these authors a similar mechanism would explain the significant isomerase activity of GSTA3-3 in the absence of GSH. In this case a water molecule would replace GSH and work as acid/base catalyst and the tyrosine residue could assist the catalysis by hydrogen bonding with the water oxygen instead of the GSH sulfur. This mechanistic scheme proposed for hGSTA3-3 would be analogous to that already demonstrated for the bacterium *Pseudomonas testosterone* that efficiently catalyzes the isomerization in Δ^5-androstene-3,17-dione. This enzyme was thoroughly investigated showing that the reaction proceeds through the formation of a dienolate intermediate obtained when the active site Asp38 residue, acting as a base, removes a proton from C4. The same residue behaves as an acid and delivers the proton to C6.[9,10] As previously outlined, it has been demonstrated that GSTs, in addition to their importance in detoxification processes, play a key-role in human steroidogenesis. In particular a direct evidence for the involvement of hGSTA3-3 in the biosynthesis of steroid hormones in human cells has been described by Mannervick and co-workers.[3,4] Polycystic ovary syndrome, congenital adrenal hyperplasia and Cushing's syndrome, for instance, are human endocrine disorders characterized by excessive steroid hormone production. Also, prostate and breast cancers are stimulated by sex steroid hormones.[11−13] This makes GSTs a possible target of great interest to pharmacologists to define therapies for steroid hormone-dependent diseases. Thus, a detailed knowledge of the reaction mechanism together with the use of transition state mimicry as a guiding design principle can be of outstanding importance to obtain new effective drugs capable of reducing steroid hormone production in human cells. In the present paper we describe the results that we have recently obtained in a computational study of the human GSTA3-3 mechanism. Considering that, as far as we know, no detailed theoretical investigations of the entire mechanism are available in literature, our goal is to elucidate some mechanistic aspects that are still obscure. In particular we try to answer the following questions: (i) Does a dienolate intermediate really exist on the reaction surface? (ii) Does the GSH molecule really behave as acid/base catalyst? (iii) What is the role of the tyrosine residue Y9? (iv) Is the contribution of other active site residues important in the catalysis? To clarify these aspects a complete investigation of the potential energy surface has been carried out using a hybrid Quantum Mechanics/Molecular Mechanics (QM/MM) approach. Furthermore, a detailed analysis (Fingerprint Analysis) has been performed within this hybrid scheme to evaluate the influence on the catalysis of the various residues surrounding the active site.

COMPUTATIONAL DETAILS

The model-system used in the present paper has been constructed starting from the coordinates of the ternary complex hGSTA3-3/GSH/Δ^5-AD kindly provided by Prof. Xinhua Ji (see ref 7). This ternary complex was obtained from the dimeric crystallographic structure of hGSTA3-3 (pdb code 1TDI) in complex with glutathione (GSH) (which was cocrystallized with the protein) by docking the substrate Δ^5-AD into the active site.[7] To build this ternary complex all water molecules in the crystal structure were excluded except for two molecules hydrogen-bonded to GSH. The model of the ternary complex hGSTA3-3/GSH/Δ^5-AD was validated both structurally and functionally.[7] For our calculations we have used the entire dimeric structure of hGSTA3-3 because the reaction takes place at the dimeric interface (Supporting Information, Figure S1). The model-system obtained from the previous ternary complex was protonated using the H++ software.[14] This code uses an automated algorithm that computes pK_a values of ionizable groups in macromolecules and adds missing hydrogen atoms according to the specified pH value of the environment. Positions of added H atoms were also optimized

dx.doi.org/10.1021/cs200369b | *ACS Catal.* 2012, 2, 280−286

by this algorithm. The protonation state of all titratable residues was carefully checked by visual inspection of the H++ output structure. The thiol group of GSH was considered deprotonated (thiolate) on the basis of available biochemical data.[6,7] The Δ^5—androstene-3,17-dione was parametrized using the Generalized Amber Force Field (GAFF).[19] Partial atomic charges were assigned to atoms using the AM1-BCC method[16] as implemented in the *antechamber* module of the AMBER8.0 package.[17] The initial model-system geometry was fully minimized at the MM level using the *sander* module of AMBER8.0.[17] The minimization was carried out with the Amber Force Field (Amber-*ff99*)[18] until the root-mean-square deviation (rmsd) of the Cartesian elements of the gradient was less than 0.0001 kcal mol^{-1}. A full conjugate gradient minimization approach and the General Born (GB)[19] model to simulate the aqueous environment (as implemented in the *sander* module of the AMBER8.0 code) were used. We carried out a Quenched Molecular Dynamics (QMD) to achieve a conformational optimization of the Michaelis complex structure. The four water molecules present in the models were retained in the calculations. A region of a 5 Å radius around the substrate was free to move during the Molecular Dynamics (MD) simulation. The system was heated from 0 to 800 K in 500 ps, and then a trajectory of 5 ns was computed at constant temperature (800 K). The integration step of 2 fs was used in conjunction with the SHAKE algorithm[20] to constrain the stretching of bonds involving hydrogen atoms. Solvent effects were taken into account using the GB model[19] with a dielectric constant of 78.5. The coordinates of the system were saved on a trajectory file every 5 ps, giving a total of 1000 structures. All the 1000 structures were fully minimized, without restraints until convergence. The lowest energy structure was considered as the best guess for the Michaelis complex, and it was used in the subsequent calculations. A cap of water molecules of radius 25 Å centered on the substrate was added (Supporting Information, Figure S1). Freezing the ternary complex to the previously obtained structure, an MD computation of 1 ns was carried out to relax the water cap. The final snapshot was minimized and used to build the model for subsequent QM/MM computations. To investigate the potential energy surface we have used a newly implemented hybrid Quantum Mechanics/Molecular Mechanics approach.[21] A special feature of our QM/MM approach is the partition of the system into three layers: the innermost layer named "High" (**H**), the outermost layer named "Low" (**L**), and an intermediate layer named "Medium" (**M**). The **H** layer is described at the QM level, while the **M** and **L** layers are both described at the MM level, but are handled differently during geometry optimization: while **H** and **M** are optimized together, **L** may be optimized independently at each **M**+**H** structure. We have demonstrated that the presence of the **M** layer effectively improves the efficiency of the geometry optimization procedure (faster optimization and higher accuracy).[21]

In QM/MM computations the atom selection to define the various layers (**H**, **M**, and **L** regions) is of primary importance to obtain a model-system which can reasonably emulate the real enzyme and provide reliable results. Thus, we have included in the **H** layer (QM region) only the molecular fragments directly involved in the enzyme-catalyzed isomerization process, that is, the side chain of the cysteine residue belonging to the tripeptide GSH, the tyrosine residue Y9 (in this case we have considered the phenolic ring fragment), and rings A and B of the steroid nucleus, and we have saturated all the dangling bonds with hydrogen atoms (atom-link approach). The GSH cysteine residue is negatively charged (deprotonated thiolate group $-CH_2-S^{(-)}$) since it should act as a base in the double bond isomerization mechanism (see the previously discussed mechanistic scheme). The tyrosine residue has been included since it has been demonstrated that the activity of hGSTA3-3 is highly dependent on the phenolic hydroxyl group.[7] The intermediate layer includes the backbone of the tyrosine residue (Y9), the remaining part of both GSH and substrate (Δ^5-AD) molecules, the arginine residue R15 and the two water molecules hydrogen-bonded to Δ^5-AD and GSH and retained from the crystallographic structure (PDB 1TDI). All the remaining water molecules and enzyme residues (described at the MM level) belong to the **L** region (the partition of our model system is shown in the Supporting Information, Figure S2. The QM/MM potential adopted in this work is based on (a) DFT/B3LYP calculations[22−26] with the double-ζ DZVP basis set[27] for all atoms of the QM region **H** and (b) the amber-*ff99* force field[18] to describe the MM atoms in the **M** and **L** regions (GAFF parameters[15] were adopted for the Δ^5-AD substrate).

As described in our previous paper[21] our approach is based on a simple Subtractive Scheme similar to that used in the two-layer ONIOM method.[21] The QM/MM potential is constructed by performing a QM single point on the QM layer, an MM single point on the same region, and an MM single point on the whole system. In our implementation the electrostatic effect of the MM region on the QM layer is taken into account by performing the QM single point calculations in the presence of all the partial atomic point charges of the MM atoms. To account for the electrostatic effect of the QM region on the MM one, in the version of the code used in this paper we have slightly modified our earlier implementation described in ref 21. Now a QM single point calculation is used to estimate both the QM wave function polarization due to the MM charges and the electrostatic forces exerted on the MM atoms by the QM electronic density. In particular the electric field and the electric potential is estimated in correspondence of each MM atom, and, thus, the electrostatic effect of the QM portion on the MM one is evaluated in terms of energy and forces ($F = E \cdot q$, where E is the electric field generated by the QM atoms and q is a MM charge).

In the following discussion this potential will be referred to as DFT(B3LYP/DZVP)/Amber-*ff99* potential. All the reported QM/MM computations were carried out using the general-purpose package **COBRAMM**,[21] which interfaces many commercially available QM and MM codes as well as some analysis routines. In the present work we used both GAUSSIAN03 (C02 version)[28] and GAUSSIAN09[29] packages to perform QM computations and the AMBER8.0[17] code for the MM calculations. In particular the GAUSSIAN09[29] code was employed for numerical frequency and IRC computations. During the geometry optimization (to locate minima and saddle-points) for the **H**+**M** region ("macroiteration") we applied the BFGS optimization algorithm implemented in the GAUSSIAN packages. For the **L** region ("microiteration") we used the "steepest descent" method from the *sander* tool of AMBER8.0. The nature of the critical points on the PES was determined by means of QM/MM numerical frequency calculations on the whole enzyme.

RESULTS AND DISCUSSION

The computed energy profile reported in Figure 1 shows that the isomerization reaction "apparently" proceeds through a

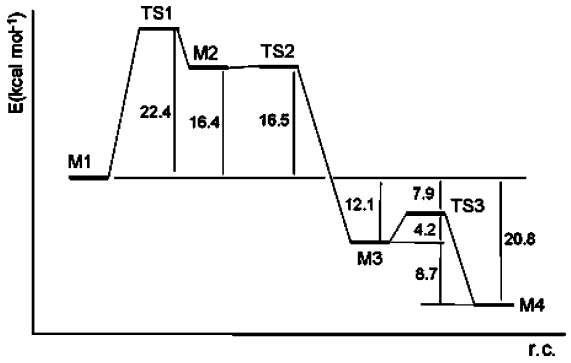

Figure 1. Energy profile obtained for the catalytic process. Energy values are given in kcal mol^{-1}.

two-step mechanism involving transition state **TS1** (with an energy barrier of 22.4 kcal mol^{-1}) and transition state **TS2** almost degenerate to the adjacent intermediate **M2**. In the former transition structure the thiolate sulfur deprotonates the C4 carbon of the Δ^5-AD substrate molecule (reactant **M1**) affording a dienolate intermediate **M2**; in the latter the tyrosine fragment Y9 releases its hydroxyl proton to C6 affording the Δ^4-AD product (**M3**). After the isomerization step a proton is easily transferred from GSH to Y9 (transition state **TS3** with an activation barrier of 4.2 kcal mol^{-1}) restoring the enzyme to its initial protonation state (**M4**). The last transformation must be very fast, being **TS3** below the asymptotic limit (**M1** reactant energy). Furthermore, the entire process is exothermic by 20.8 kcal mol^{-1}.

The four critical points **M1**, **TS1**, **M2**, and **M3** are schematically represented in Figure 2 (**M1** and **TS1**) and Figure 4 (**M2** and **M3**). To better illustrate the most important structural features of these points, only the QM portion, the arginine residue R15, and the water molecule WAT448 included in the MM region (**M** layer) are reported. Since in these figures we have adopted a two-dimensional representation, several atomic distances appear much longer (or shorter) than in the real protein. A more realistic three-dimensional picture of the four critical points is also given in Figure 2 and Figure 4 (right side).

In **M1** the thiolate sulfur of GSH is positioned at 3.69 and 5.13 Å from C4 and C6, respectively, and the hydroxyl hydrogen of Y9 is at 2.66 Å from C6. The ε-hydrogen of R15 participates in a hydrogen bond with the thiolate sulfur, the S···HN(R15) distance being 2.77 Å. Another hydrogen bond involves the hydroxyl group of Y9 and the amidic nitrogen of R15 ((R15)N···HO(Y9) distance = 1.98 Å). Furthermore, a hydrogen bond is evident between WAT448 and the substrate carbonyl oxygen, the (WAT448)H···O distance being 2.33 Å. The same water molecule is involved in a second hydrogen bond with the GSH tripeptide molecule: in this case the water oxygen interacts with the N−H group of the peptide bond between glycine and cysteine (O···NH(GSH) distance = 1.89 Å). These structural features are in good agreement with the crystallographic structure of hGSTA3-3·GSH obtained by Ji and co-workers[7] and the model of the hGSTA3-3·GSH·Δ^5-AD ternary complex constructed by these authors. At the transition state **TS1** a proton is moving from C4 to the thiolate sulfur

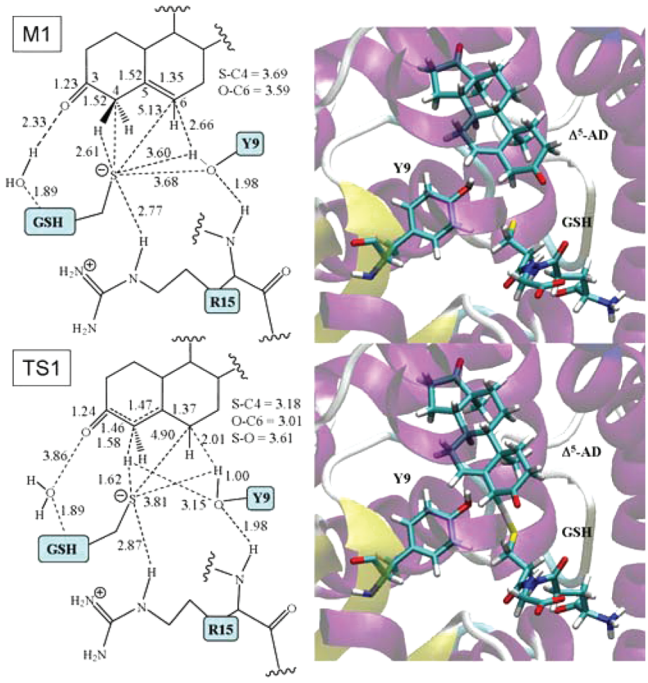

Figure 2. Two-dimensional (left) and three-dimensional (right) representation of the structure of the two critical points **M1** and **TS1** (bond lengths in angstroms).

(the C4···H and H···S distances are 1.58 and 1.62 Å, respectively) and the Y9 hydroxyl group is closer to C6, the H···C6 distance being now 2.01 Å. Interestingly, the two C3−C4 and C4−C5 bonds become almost equivalent (1.46 and 1.47 Å, respectively), which clearly indicates the delocalization of the π bond determined by the loss of a proton at the C4 carbon. The involvement of the C5−C6 bond in the delocalization is negligible: this bond distance is 1.37 Å, which is only slightly longer than the corresponding value in **M1** (1.35 Å). Also, the hydrogen bond between the substrate carbonyl oxygen and the water molecule disappears, the distance between the WAT448 oxygen and the carbonyl oxygen being now 3.86 Å. This is caused by the strong hydrogen bond between WAT448 and the cysteine NH group of GSH: since during the proton transfer this residue changes its position, it can maintain the hydrogen bond with WAT448 at the expense of the interaction (that disappears) between WAT448 and the carbonyl oxygen.

To obtain more detailed information on the reaction pathway we have carried out Intrinsic Reaction Coordinate (IRC) computations starting from **TS1** and moving in both reactant (**M1**) and product (**M2**) direction. The computed potential energy curve and the change of the two main geometrical parameters (C4−H distance and S−H distance) are reported in Figure 3. These results establish for certain the connection of **TS1** with **M1** and the **M2** region.

The subsequent intermediate **M2** (16.4 kcal mol^{-1} above **M1**) resembles the dienolate intermediate of Scheme 1 proposed by Ji and co-workers.[7] Here the proton transfer to the thiolate group is complete, and the π system is fully delocalized along the O−C3−C5−C5−C6 framework, as clearly indicated by the CO and CC distances (C−O, C3−C4, C4−C5, and C5−C6 are 1.26, 1.43, 1.40, and 1.41 Å, respectively). However, before confirming the existence of a dienolate intermediate, it is worth taking into account the

dx.doi.org/10.1021/cs200369b | ACS Catal. 2012, 2, 280−286

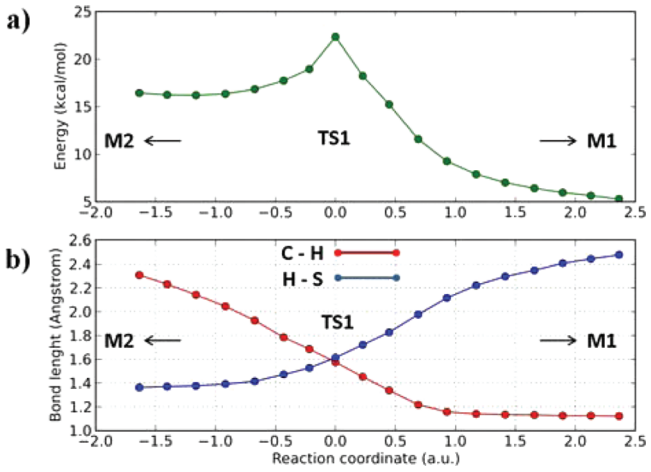

Figure 3. Diagram that illustrates the results of the Intrinsic Reaction Coordinate (IRC) computations. (a) Energy trend in the reactant (**M1**) and product (**M2**) direction. (b) Variations of the two main geometrical parameters (C4−H distance, red line and S−H distance, blue line) describing the reaction coordinate.

energy and structure of the following transition state **TS2** which should complete the isomerization by transferring a proton from the Y9 hydroxyl group to C6. The structure of **TS2** (schematically represented in the Supporting Information, Figure S3) is very close to that of **M2** and is almost degenerate to it (it is only 0.1 kcal mol^{-1} higher than **M2**). Here the proton transfer process is at the beginning, and the hydrogen is still strongly bonded to the Y9 oxygen, the OH and H···C6 distances being 1.09 and 1.70 Å, respectively. This suggests that the dienolate intermediate actually corresponds to an extremely flat region of the potential surface which does not prove the existence of a real intermediate.

The double bond isomerization is entirely accomplished in the product **M3**, where the C4−C5 and C5−C6 distances are 1.35 and 1.51 Å, respectively. Here the sulfur-bonded proton strongly interacts with the Y9 negative oxygen, the S−H···O distance being 2.06 Å.

This strong hydrogen bond anticipates the proton transfer occurring in the subsequent fast step (**M3** → **TS3** → **M4**), which restores the enzyme to its initial state. A schematic representation of **TS3** and **M4** is given in the Supporting Information, Figures S3 and S4. Interestingly, in the final product **M4**, when the GSH cysteine, after having fulfilled its catalytic cycle, can approximately reach the original position occupied in **M1**, the water molecule can move again toward the carbonyl substrate and restore the initial hydrogen bond ((WAT448)H···O distance =2.37 Å). This stabilizing hydrogen interaction is certainly an important factor that contributes to lower the energy of **M4** together with the resonance effect of the new CC double bond (Δ^4) conjugated with the carbonyl fragment.

An additional structural feature that is worth highlighting is the hydrogen bond involving the ε nitrogen of R15 and the thiolate group of GSH: the S···H−N(ε) distances are 2.77, 2.87, 2.77, and 2.71 Å in **M1**, **TS1**, **M2**, and **M3**, respectively (see Figure 2 and Figure 4). This hydrogen bond is a sign of the role played by arginine in stabilizing the thiolate group of GSH as suggested by Ji and co-workers[7] (see the following discussion concerning the Fingerprint Analysis). An additional and stronger hydrogen bond involving the hydroxyl group of tyrosine (Y9) and the α N−H group of R15 contributes to

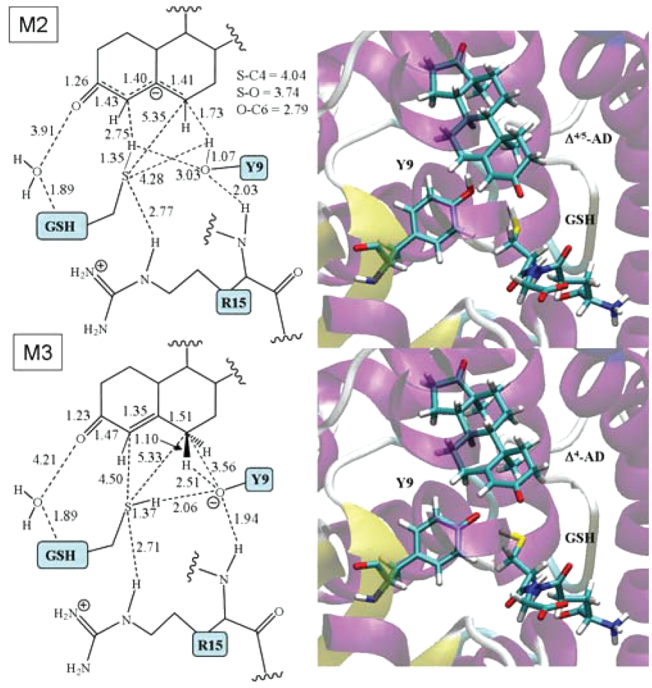

Figure 4. Two-dimensional (left) and three-dimensional (right) representation of the structure of the two critical points **M2** and **M3** (bond lengths in angstroms).

stabilize the reacting system. It is interesting to compare the structural features of **M3** with the crystallographic data recently obtained by Mannervik for hGSTA3-3 in complex with Δ^4-AD.[9] The computed values for the C6···O(Y9) and C4···S-(GSH) distances are 3.56 and 4.50 Å, respectively, which are in reasonable agreement with the crystallographic values of 4.0 and 3.7 Å. The computed (GSH)S···O(Y9) distance (3.43 Å) is also close enough to the experiment (3.0 Å). The most significant difference is found for the (GSH)S···C6 distance, the computed and experimental values being 5.33 and 3.5 Å, respectively. However, the discrepancy between theory and experiment could be reduced by a dynamical treatment (and not a simple minimization) of the structure of the product intermediate **M3**.

In summary our computations indicate that the catalytic process leading from Δ^5-AD to Δ^4-AD is actually a highly asynchronous concerted process (and only "apparently" a two-step reaction) where the migration of the two protons occurs in two different phases: first from C4 to the thiolate sulfur and then, after leaving behind a wide flat region corresponding to a dienolate-type structure, from the Y9 hydroxyl group to C6. In spite of extensive search we have not found any evidence for a genuine stepwise mechanism involving the formation of a real dienolate intermediate. Interestingly, a pronounced hole for this transient species does not exists on the reaction surface although we have included in our QM model a water molecule which should stabilize the possible dienolate intermediate. The existence of this intermediate species probably requires a stronger stabilization such as that of the oxyanion hole which is present in the enzyme isolated from the bacterium *P. testosteroni* and not in hGSTA3-3.[30] Furthermore, the suggestion of Mannervick and co-workers[5,9] that the GSH cofactor acts as base/acid catalyst is basically in agreement with our computational finding: in the first step (**M1**→ **M3**) the GSH thiolate behaves as a base and captures a proton from C4 and in the

dx.doi.org/10.1021/cs200369b | *ACS Catal.* 2012, 2, 280−286

second step (**M3** → **M4**) it acts as an acid and gives back the proton to tyrosine. Since the second step has a very low barrier and the energy of **TS3** is lower than reactants, we could consider the entire process (i.e., the whole energy profile of Figure 1) as a single very asynchronous proton transfer governed by GSH and "assisted" by tyrosine that behaves as a proton shuttle. The role of tyrosine is essential because the sulfur atom remains too far away from C6 to allow a direct proton transfer to this carbon (the S···C6 distance is 5.13 and 4.90 Å in **M1** and **TS1**, respectively). This can be accomplished much more easily with the help of the tyrosine residue which can approach ring B of the steroid nucleus (the C6···H distance in **TS1** is only 2.01 Å).

We have rationalized the electrostatic effects on the catalysis of the various residues surrounding the active site. Our analysis (named "Fingerprint Analysis" and illustrated in details in refs 31 and 32) allows a ranking of the electrostatic effects of the single residues. In this way it is possible to identify the most important residues determining the relative stabilization/destabilization of two critical points: for instance, **M1** and **TS1** in the present case. This procedure provides information on the effects of each residue on the entity of the activation barrier. The results of our analysis are schematically represented in the diagram of Figure 5 where we report the stability

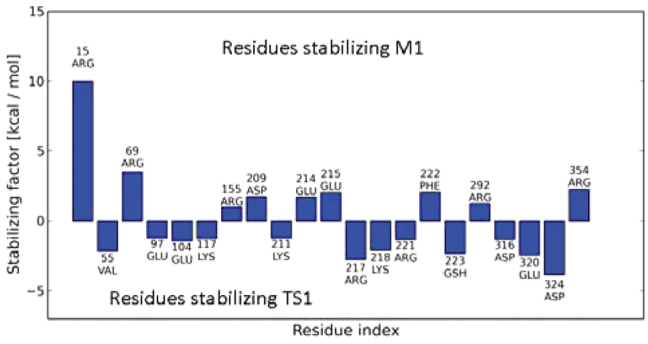

Figure 5. Fingerprint analysis for the comparison **M1**-**TS1**. The stability parameter **S** is reported as a function of the various residues.

parameter **S** as a function of the various residues (including water molecules) within 10 Å from the QM region. Positive and negative S values indicate stabilization of **M1** and **TS1**, respectively (or, alternatively, destabilization of **TS1** and **M1**).[25,26]

It is evident from the diagram that the major contribution to the **M1** stabilization is due to the arginine residue R15. Inspection of Figure 2 shows that after the proton transfer from Δ^5-AD to the GSH thiolate group the hydrogen bond between the sulfur atom and the ε nitrogen of R15 becomes weaker: the S···H−N(ε) distance varies from 2.77 to 2.87 Å on passing from **M1** to **TS1** and the charge on S decreases from −0.93 to −0.72 in the same direction. Another important factor that explains the large contribution of arginine is the effective hydrogen bond involving the hydroxyl group of tyrosine (Y9) and the α N−H group of R15. These structural features are in agreement with the strong contribution of R15 to the **M1** stabilization as highlighted by the fingerprint analysis. Moreover, the stabilization due to this hydrogen bond explains the existence of a thiolate (deprotonated cysteine sulfur) in the active site.

The fingerprint analysis has also evidenced other residues (with weaker contributions) which are responsible for electrostatic effects that stabilize **M1** or **TS1**. For instance, additional long-range stabilizing effects on **M1** are due to Arg-69 and Arg-354, while other positively charged residues, such as Arg-217, Arg-221, Lys-211, and Lys-218 contribute to stabilize **TS1** by interacting with the delocalized negative charge of the transition state.

CONCLUSION

In this paper we have carried out a detailed computational investigation at the QM/MM level of the catalytic mechanism of the human glutathione transferase A3-3 (hGSTA3-3). The most relevant results can be summarized as follows:

(i) The isomerization reaction is only "apparently" a two-step process. Actually, the reaction is characterized by a concerted highly asynchronous mechanism (two-phase process) where at first the C4 carbon of Δ^5-AD (substrate) is deprotonated by the GSH thiolate sulfur (acting as a base) and, then, the hydroxyl proton of the tyrosine fragment Y9 is transferred to C6 affording the Δ^4-AD product. In a second step characterized by a rather low barrier (only 4.2 kcal mol^{-1}) the initial state of the enzyme can be restored by transferring a proton from the GSH sulfur (acting as an acid) to the tyrosine negative oxygen.

(ii) We have not found any evidence for a "genuine" stepwise mechanism involving the formation of a real dienolate intermediate featured by a well "pronounced hole" on the potential surface. Our computations demonstrate that GSH acts as a base/acid catalyst and governs the proton transfer from C4 to C6 (a mechanism in some way similar to that hypothesized by Mannervik[5,9]). However this process requires the participation of the tyrosine residue Y9 that behaves as a proton shuttle and effectively "assists" the proton transfer. Our results show that the GSH sulfur atom is too far away from C6 (5.13 Å in **M1** and 5.33 Å in **M3**) to transfer directly a proton back to ring B of the steroid nucleus. Also, the SH group does not have the structural freedom required to move close enough to C6 and make the proton transfer possible.

(iii) The structural features of **M1** (starting complex) are in good agreement with those of the hGSTA3-3·GSH·Δ^5-AD ternary complex constructed by Ji and co-workers[7] who docked the substrate into the active site of the crystal structure of hGSTA3-3·GSH they had previously obtained. A fair agreement has been also found in the comparison between **M3** and the crystal structure recently determined by Mannervik[9] for GST A3-3 in complex with GSH and the product of the steroid isomerization Δ^4-AD.

(iv) We have clearly demonstrated the key role played by arginine R15 in stabilizing the reacting system. This stabilization is mainly due to a hydrogen bond between the GSH thiolate group and the ε nitrogen of R15 as hypothesized by Ji and co-workers.[7] A further stabilizing H-bond is that involving the hydroxyl group of tyrosine (Y9) and the α N−H group of R15.

(v) We have used a "fingerprint analysis" to rank the electrostatic effects on the catalysis of the various residues surrounding the active site. This analysis has evidenced the major contribution of the arginine residue R15 in stabilizing the initial complex **M1**, in agreement

dx.doi.org/10.1021/cs200369b | ACS Catal. 2012, 2, 280−286

with the structural features previously discussed for the hydrogen bonds involving R15, GSH, and Y9. Long-range stabilizing effects on **TS1** are due to Arg-217, Arg-221, Lys-211, and Lys-218 that contribute to stabilize **TS1** by interacting with the delocalized negative charge of the transition state.

■ ASSOCIATED CONTENT

Supporting Information

Dimeric structure of hGSTA3-3; schematic representation of the partition of the model-system used in this study; two-dimensional schematic representation of the structure of the critical points **TS2**, **TS3**, and **M4**; three-dimensional representation of the structure of the three critical points **TS2**, **TS3**, and **M4**. Cartesian coordinates of the atoms belonging to the **H** and **M** regions for the seven critical points **M1**, **TS1**, **M2**, **TS2**, **M3**, **TS3**, **M4** located on the potential energy surface. This material is available free of charge via the Internet at http://pubs.acs.org.

■ AUTHOR INFORMATION

Corresponding Author

*E-mail: marco.stenta@epfl.ch (M.S.). E-mail: andrea.bottoni@unibo.it (A.B.).

■ REFERENCES

(1) Sheehan, D.; Meade, G.; Foley, V. M.; Dowd, C. A. *Biochem. J.* **2001**, *360*, 1−16.
(2) Hayes, J. D.; Flanagan, J. U.; Jowsey, I. R. *Annu. Rev. Pharmacol. Toxicol.* **2005**, *45*, 51−88.
(3) Johnsson, A. S.; Mannervik, B. *J. Biol. Chem.* **2001**, *276*, 33061−33065.
(4) Raffalli-Mathieu, F.; Orre, C.; Stridsberg, M.; Hansson Edalat, M.; Mannervik, B. *Biochem. J.* **2008**, *414*, 103−109.
(5) Petterson, P. L.; Johnsson, A. S.; Mannervik, B. *J. Biol. Chem.* **2002**, *277*, 30019−30022.
(6) Johansson, A.-S.; Mannervik, B. *J. Biol. Chem.* **2002**, *277*, 16648−16654.
(7) Gu, Y.; Guo, J.; Pal, A.; Pan, S.-S.; Zimniak, P.; Singh, S. V.; Ji, X. *Biochemistry* **2004**, *43*, 15673−15679.
(8) Sinning, I.; Kleywegt, G. J.; Cowan, S. W.; Reinemer, P.; Dirr, H. W.; Huber, R.; Gilliland, G. L.; Armstrong, R. N.; Ji, X.; Board, P. G.; Olin, B.; Mannervik, B.; Jones, T. A. *J. Mol. Biol.* **1993**, *232*, 192−212.
(9) Tars, K.; Olin, B.; Mannervik, B. *J. Mol. Biol.* **2010**, *397*, 332−340.
(10) Talalay, P.; Wang, V. S. *Biochim. Biophys. Acta* **1955**, *18*, 300−301.
(11) Chang, R. *Am. J. Obstet. Gynecol.* **2004**, *191*, 713−717.
(12) Newell-Price, J.; Bertagna, X.; Grossman, A. B.; Nieman, L. K. *Lancet* **2006**, *367*, 1605−1617.
(13) Henderson, B. E.; Feigelson, H. S. *Carcinogenesis* **2000**, *21*, 427−433.
(14) Gordon, J. C.; Myers, J. B.; Folta, T.; Shoja, V.; Heath, L. S.; Onufriev, A. *Nucleic Acids Res.* **2005**, *33*, 368−371.
(15) Wang, J.; Wolf, R. M.; Caldwell, J. W.; Kollman, P. A.; Case, D. A. *J. Comput. Chem.* **2004**, *25*, 1157−1174.
(16) Jakalian, A.; Bush, B. L.; Jack, D. B.; Bayly, C. I. *J. Comput. Chem.* **2000**, *21*, 132−146.
(17) Case, D. A.; Cheatham, T. E.; Darden, T.; Gohlke, H.; Luo, R.; Merz, K. M.; Onufriev, A.; Simmerling, C.; Wang, B.; Woods, R. J. *J. Comput. Chem.* **2005**, *26*, 1668−1688.
(18) Ponder, J. W.; Case, D. A.; Valerie, D. In *Advances in Protein Chemistry*; Academic Press: New York, 2003; Vol. *66*, pp 27−85.
(19) Onufriev, A.; Bashford, D.; Case, D. A. *J. Phys. Chem. B* **2000**, *104*, 3712−3720.
(20) Ryckaert, J.-P.; Ciccotti, G.; Berendsen, H. J. C. *J. Comput. Phys.* **1977**, *23*, 327−341.
(21) Altoè, P.; Stenta, M.; Bottoni, A.; Garavelli, M. *Theor. Chem. Acc.* **2007**, *118*, 219−240.
(22) Becke, A. D. J. *J. Chem. Phys.* **1993**, *98*, 1372−1377.
(23) Calvaresi, M.; Bottoni, A.; Garavelli, M. *J. Phys. Chem. B* **2007**, *111*, 6557−6570.
(24) Calvaresi, M.; Bottoni, A.; Garavelli, M. *Proteins* **2008**, *73*, 527−538.
(25) Miscione, G. P.; Calvaresi, M.; Bottoni, A. *J. Phys. Chem. B* **2010**, *114*, 4637−4645.
(26) Bottoni, A.; Miscione, G. P.; Calvaresi, M. *Phys. Chem. Chem. Phys.* **2011**, *13*, 9568−9577.
(27) Godbout, N.; Salahub, D. R.; Andzelm, J.; Wimmer, E. *Can. J. Chem.* **1992**, *70*, 560−571.
(28) Frisch, M. J.; Trucks, G. W.; Schlegel, H. B.; Scuseria, G. E.; Robb, M. A.; Cheeseman, J. R.; Montgomery, Jr., J. A.; Vreven, T.; Kudin, K. N.; Burant, J. C.; Millam, J. M.; Iyengar, S. S.; Tomasi, J.; Barone, V.; Mennucci, B.; Cossi, M.; Scalmani, G.; Rega, N.; Petersson, G. A.; Nakatsuji, H.; Hada, M.; Ehara, M.; Toyota, K.; Fukuda, R.; Hasegawa, J.; Ishida, M.; Nakajima, T.; Honda, Y.; Kitao, O.; Nakai, H.; Klene, M.; Li, X.; Knox, J. E.; Hratchian, H. P.; Cross, J. B.; Bakken, V.; Adamo, C.; Jaramillo, J.; Gomperts, R.; Stratmann, R. E.; Yazyev, O.; Austin, A. J.; Cammi, R.; Pomelli, C.; Ochterski, J. W.; Ayala, P. Y.; Morokuma, K.; Voth, G. A.; Salvador, P.; Dannenberg, J. J.; Zakrzewski, V. G.; Dapprich, S.; Daniels, A. D.; Strain, M. C.; Farkas, O.; Malick, D. K.; Rabuck, A. D.; Raghavachari, K.; Foresman, J. B.; Ortiz, J. V.; Cui, Q.; Baboul, A. G.; Clifford, S.; Cioslowski, J.; Stefanov, B. B.; Liu, G.; Liashenko, A.; Piskorz, P.; Komaromi, I.; Martin, R. L.; Fox, D. J.; Keith, T.; Al-Laham, M. A.; Peng, C. Y.; Nanayakkara, A.; Challacombe, M.; Gill, P. M. W.; Johnson, B.; Chen, W.; Wong, M. W.; Gonzalez, C.; and Pople, J. A. *Gaussian 03*, Revision C.02; Gaussian, Inc.: Wallingford, CT, 2004.
(29) Frisch, M. J.; Trucks, G. W.; Schlegel, H. B.; Scuseria, G. E.; Robb, M. A.; Cheeseman, J. R.; Scalmani, G.; Barone, V.; Mennucci, B.; Petersson, G. A.; Nakatsuji, H.; Caricato, M.; Li, X.; Hratchian, H. P.; Izmaylov, A. F.; Bloino, J.; Zheng, G.; Sonnenberg, J. L.; Hada, M.; Ehara, M.; Toyota, K.; Fukuda, R.; Hasegawa, J.; Ishida, M.; Nakajima, T.; Honda, Y.; Kitao, O.; Nakai, H.; Vreven, T.; Montgomery, Jr., J. A.; Peralta, J. E.; Ogliaro, F.; Bearpark, M.; Heyd, J. J.; Brothers, E.; Kudin, K. N.; Staroverov, V. N.; Kobayashi, R.; Normand, J.; Raghavachari, K.; Rendell, A.; Burant, J. C.; Iyengar, S. S.; Tomasi, J.; Cossi, M.; Rega, N.; Millam, N. J.; Klene, M.; Knox, J. E.; Cross, J. B.; Bakken, V.; Adamo, C.; Jaramillo, J.; Gomperts, R.; Stratmann, R. E.; Yazyev, O.; Austin, A. J.; Cammi, R.; Pomelli, C.; Ochterski, J. W.; Martin, R. L.; Morokuma, K.; Zakrzewski, V. G.; Voth, G. A.; Salvador, P.; Dannenberg, J. J.; Dapprich, S.; Daniels, A. D.; Farkas, Ö.; Foresman, J. B.; Ortiz, J. V.; Cioslowski, J.; Fox, D. J. *Gaussian 09*, Revision A.02; Gaussian, Inc.: Wallingford, CT, 2009.
(30) Gerlt, J. A.; Gassman, P. G. *Biochemistry* **1993**, *32*, 11934−11952.
(31) Stenta, M.; Calvaresi, M.; Altoè, P.; Spinelli, D.; Garavelli, M.; Bottoni, A. *J. Phys. Chem. B* **2008**, *112*, 1057−1059.
(32) Stenta, M.; Calvaresi, M.; Altoè, P.; Spinelli, D.; Garavelli, M.; Galeazzi, R.; Bottoni, A. *J. Chem. Theory Comput.* **2009**, *5*, 1915−1930.